100 kWe Magnetoplasmadynamic Thruster System Design

L.K. Rudolph*
Martin Marietta Corporation, Denver, Colorado

and

D.Q. King†
Jet Propulsion Laboratory, California Institute of Technology, Pasadena, California

A magnetoplasmadynamic (MPD) thruster system point design is presented that may be applicable to a wide variety of future space missions. The system is electrically matched to a 100 kWe nuclear thermoelectric supply and operates the thruster in a pulsed, quasisteady mode on cryogenically stored argon. The overall system efficiency is 52% which includes efficiencies of the electrolytic capacitor energy store, constant power charging unit, and thyristor switch, and assumes a 60% thruster efficiency. The system specific mass is 21.6 kg/kWe. Various technology improvements are discussed which could reduce the specific mass to under 10 kg/kWe, while simultaneously increasing the efficiency and reducing the overall system complexity.

Introduction

THE promise of electric propulsion—large total impulse with minimal reaction mass—has prompted the development of several completely different electric engines and the design of many spacecraft using these thrusters. Applicable missions range from Earth orbital transfers to planetary exploration, and require thrusters consuming any amount from a few watts to a few megawatts of power.[1,2] One of the most promising engines currently under active development is the multimegawatt, pulsed, quasisteady, self-field, magnetoplasmadynamic (MPD) thruster.[3] This paper describes a 100 kWe propulsion system design for this thruster that is suited for applications ranging from Earth orbit transfer to planetary exploration. This design was developed to assess to first order the characteristics of a 100 kWe, pulsed, MPD thruster system as a part of a continuing effort to better understand the place of MPD thruster systems in future space programs.

System Overview

An overall design concept for a nuclear electric propulsion (NEP) vehicle is shown in Fig. 1. This system includes a 1.4 MWt SP-100 reactor, a 100 kWe thermoelectric converter/radiator, an MPD thruster system, and a payload. Here in the so called side-thrust configuration, the thruster acts on a vector perpendicular to the major axis of the spacecraft. Figure 1 shows the vehicle with its payload in the stowed configuration. During thruster operation, the payload is extended out 11 m by an astromast assembly as required to position the spacecraft center of mass on the thrust vector. This particular design is for a Neptune orbiter mission, which represents one of the most challenging applications for this vehicle class. This mission was chosen as the baseline for this design for this reason and because a large amount of data has already been generated in companion studies concerning the overall mission trajectory, propellant requirements, Earth launch operations, etc.[4] This vehicle is designed to be compatible with, and deployed by, the Space Shuttle in a 700-km altitude, nuclear quarantine, Earth orbit.

A schematic block diagram of the MPD thruster system is shown in Fig. 2. It includes all those components necessary to accept raw power from the nuclear thermoelectric supply and convert it into thrust on command. The primary power train consists of the charging power processor/conditioner, energy storage, high current/power pulse switch, and MPD thruster. In parallel with this power train is the propellant storage and handling subsystem consisting of the primary propellant storage tank, control valves and pressure regulators, plenum storage reservoir chamber, high speed pulse valves, and, again, the MPD thruster. The remaining system components and overall structure serve to support and control the operation of these primary system activities.

To provide an overall context for the more detailed analyses to follow, a brief summary description of this system is included here. The thruster design used in this system is projected from characteristics that are typical of existing laboratory hardware.[5] Argon propellant is used for this thruster primarily due to its well understood behavior in the MPD discharge; however, its relatively benign chemical properties and ease of manufacture and handling suggest that it could easily be advantageous for many future missions. The thruster discharge propellant flow rate is projected to be 2.2 g/s or 11 mg/pulse for the baselined 5 ms pulse duration. The peak thruster power is 4 MWe, leading to a pulse rate of 4.4 Hz at 100 kWe input, after accounting for the various system inefficiencies. To carry a modest payload to Neptune orbit, 9116 kg of argon propellant are required, providing a total impulse of 5.08×10^8 N-s.[4] The propellant is stored as a cryogenic liquid at a temperature of 90 K in a well insulated spherical tank located with its center of mass lying directly on the thrust vector, immediately forward of the main thruster system, as can be seen in Fig. 1. Radiative cooling through the propellant tank wall is sufficient to maintain the argon in a liquid state for the entire mission duration.

During thruster system operation, a small amount of electrical heat generated in the propellant tank provides sufficient argon vapor to supply the thruster. This argon flows through a pressure regulator to a plenum chamber immediately upstream of an array of six parallel, high-speed solenoid valves. These valves are closely coupled to the thruster discharge chamber such that the argon flows into the chamber in a square pulse of 5 ms duration. The argon flow rate is controlled via choked flow through small injection orifices in the valves. The plenum chamber is sized such that the pressure upstream of these orifices remains essentially constant during the pulse duration.

The outer wall of the propellant plenum chamber is connected to the thruster anode (Fig. 3) and forms the outgoing

Presented as Paper 82-1897 at the AIAA/JSASS/DGLR 16th International Electric Propulsion Conference, New Orleans, La. Nov. 17–19, 1982; received March 24, 1983; revision received Sept. 18, 1983.

*Senior Staff Engineer, Propulsion Section. Member AIAA.

†Senior Engineer, Electric Propulsion and Plasma Technology Group. Member AIAA.

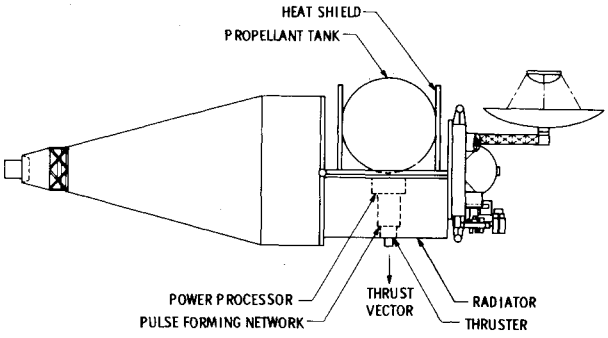

Fig. 1 NEP spacecraft (top view).

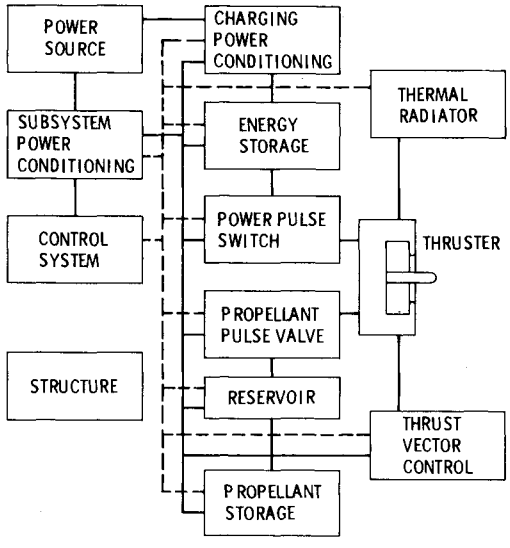

Fig. 2 MPD thruster system block diagram.

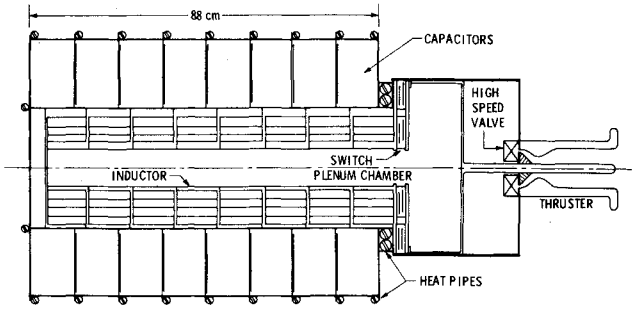

Fig. 3 Thruster/switch/PFN assembly.

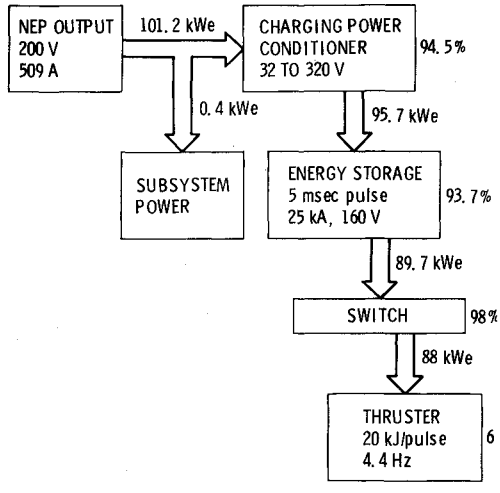

Fig. 4 System power train.

current path to the thruster. The return path flows from the cathode through the switch and energy store, both of which are inside the pressurized plenum. The switch consists of sixteen silicon controlled rectifiers (SCR's) mounted in parallel between two circular plates. It connects the thruster cathode to the output inductor of an eight-stage inductive-capacitive (L-C) ladder pulse forming network (PFN) shown in cross section in Fig. 3. This PFN is configured to supply 25 kA of thruster current at 160 V in a pulse matched to the 5-ms duration propellant pulse. Each PFN stage consists of a four-turn "jelly roll" type inductor surrounded by an axisymmetric distribution of electrolytic capacitors. As a safety measure, each capacitor stage is divided into six individually fused elements, which can be isolated from the main circuit in the event of a capacitor failure.

Roughly 10% of the total electric power delivered to the thruster is converted into heat in the electrodes.[6] The great majority of this heat is radiated into space from the high-temperature anode outer surface. The remainder is conducted into the propellant plenum chamber walls, where part is radiated into space (albeit at a much reduced temperature) and the rest is conducted upstream to the high current switch. This conducted heat, along with contributions from the switch and the PFN ohmic losses, is carried to a relatively low-temperature (roughly 78°C) radiator through a series of heat pipes surrounding the switch and PFN. This radiator and a similar radiator for the charging power processor are each configured such that they view regions of space normal to both the flight direction and the spacecraft longitudinal axis. This configuration minimizes any radiator impingement by either solar or Earth radiation and so maximizes the radiated power. As shown in Fig. 1, these radiators are located both above and below the thruster system, where they are easily accessible by the heat pipes from the system components.

The remaining system components have been examined in less detail in this study because of limitations on the study itself and because they are already relatively well understood through their similarity to components of other flight systems. The charging power processor serves to convert the steady thermoelectric converter output at 200 Vdc to a continuously repeating sawtoothlike voltage ramp output which charges the PFN capacitors at a constant input power from 0 to 320 V.

The system design process consisted of making initial assumptions about each component's performance to develop an estimate of the system power input to the thruster and the resultant overall pulse rate. From these estimates, detailed designs of the various components were developed, starting with the thruster and moving up the system electrical power train to the thermoelectric converter. Slight inaccuracies in the initial component performance assumptions resulted in a final design which requires 101.6 kWe, rather than the assumed 100 kWe, which is well within the overall design uncertainty. The final overall power train efficiency chain for the MPD system is shown in Fig. 4, where it can be seen that roughly 86% of the total electrical power is output to the thruster. Of this, 60% is assumed to be converted into thrust power for a total system efficiency of 52%.

Components

Thruster

In light of the rapid progress in developing more efficient MPD thruster designs, it is virtually impossible to select an existing thruster that would represent the ultimate flight design. Rather than so doing, a conceptual thruster design was developed through extrapolation of existing designs and an application of the theoretical understanding of the thruster

discharge.[7,8] This conceptual thruster was selected to allow a more careful design of the remaining system components, and will itself evolve as thruster development continues. A detailed sketch of this thruster is shown in Fig. 5. As can be seen, this design consists of three major parts: a fairly massive and internally contoured anode, an insulator at the upstream end of the discharge chamber which is also contoured to channel the propellant flow, and a simple cylindrical cathode.

Table 1 lists the projected operating characteristics of this thruster. These characteristics were determined assuming a 5-ms argon propellant pulse with a linear rise time of 0.3 ms and a similar fall. The discharge current pulse is also assumed to be 5 ms in duration; however, its rise and fall profiles are designed to be quadratic with time such that the ratio of discharge current squared to the mass flow rate ($J^2/\dot{m}$) is at any instant fixed. This requirement leads directly to an exhaust velocity pulse that is essentially perfectly square, since the exhaust velocity is, to the first order, proportional to $J^2/\dot{m}$. The small but finite rise and fall times of the propellant and discharge current pulses degrade the overall thrust efficiency by an amount estimated from known thruster performance data to be roughly equivalent to a 5% drop in the peak thrust efficiency. It should be noted from Table 1 that although the thruster losses are 40% of the input power, only 10% of this power appears as electrode losses while the remaining 30% is carried downstream in propellant frozen flow.

The downstream face of the anode extends out to a radius of 10 cm to provide an electrode area for the discharge current which flows downstream of the anode exit plane. The upstream anode thickness is 2 cm to minimize its thermal conductance. At the thruster base, the anode is bolted to a flat plate which extends radially outward and acts as a large conductively coupled cooling fin as well as the anode lead from the PFN.

Perhaps the greatest area of uncertainty in MPD thruster performance lies in its ultimate lifetime. Very early studies of 30-kWe steady-state MPD thrusters suggest that lifetimes well in excess of 500 h may be possible, while recent Soviet tests on applied field thrusters at comparable operating conditions suggest up to 1000 h are attainable.[9,10] One thousand hours represent roughly 8×10^8 5-ms pulses. For the purposes of this report, the thruster lifetime will be assumed to be sufficient for the baselined Neptune orbiter mission, which requires 8.3×10^8 pulses. As more accurate thruster erosion data become available, redundant thrusters can be added to the system if the individual thruster lifetime proves to be insufficient.

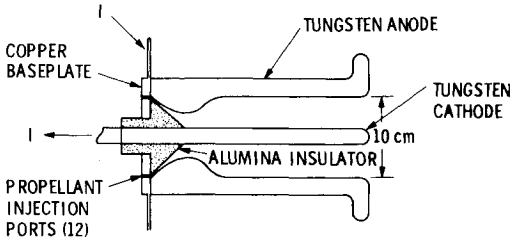

Fig. 5 Thruster cross section.

Table 1 Projected MPD thruster characteristics

Discharge current	25 kA
Propellant flow rate	2.2 g/s (argon)
Discharge voltage	160 V
Pulse power	4 MWe
Pulse duration	5 ms
Pulse energy	20 kJ
Electromagnetic thrust	101 N
Electrothermal thrust	5 N
Total thrust	106 N
Thrust power	2.6 MWe
Peak thrust efficiency	65%
Average thrust efficiency	60%
Specific impulse	5000 s
Peak heat loss to anode	0.4 MWe
Peak heat loss to cathode	Less than 0.04 MWe

Propellant Storage and Handling

Storage

For the baselined Neptune orbiter mission, the total trip time is roughly 4400 days.[4] The thruster is operated initially to accelerate the spacecraft out of Earth orbit for a burn time of 1538 days. This is followed by a coast phase, and, finally, a deceleration and orbit injection phase where the thruster is operated for roughly 500 days. The actual planetary exploration will require additional maneuvers totaling some 148 days of burn, for a total burn time of 2179 days. At a pulse rate of 4.4 Hz and using 11 mg/pulse of propellant, 9116 kg of argon is required to meet this burn time.

The design for the propellant storage system is derived from a flight weight, 16,301 kg liquid argon tank.[11] The characteristics of the storage system for the MPD-NEP vehicle can be developed by scaling down this large system from 16,301 kg to 9116 kg of stored argon. For a 95% loaded tank, this requires a 7.0 m^3 tank volume with an inner diameter of 2.37 m. The masses of the tank, insulation, and propellant acquisition device are taken to scale with the tank surface area, while the support structure is assumed to scale with the tank volume. The thermodynamic vent system/vapor cooled shield (TVS/VCS) components remain unchanged. The total storage subsystem mass breakdown for the MPD thruster system is detailed in Table 2. Also shown are the masses of those components required to fill and vent the tank and to control the propellant flow to the MPD thruster propellant plenum chamber. A schematic of the propellant storage and handling system is shown in Fig. 6.

The worst case heat load into the 9116 kg tank is 0.086 W, which corresponds to a vaporization and vent rate of 0.074 kg/h. During MPD system operation, the required argon propellant flow rate is 0.175 kg/h; thus, additional heat will be required to drive this flow. A heater is installed in the tank for this purpose and sized to vaporize the entire 0.175 kg/h. This required heat load is 0.21 W, which is insignificant and will be ignored in the overall power balance for this system design.

The baseline Neptune orbiter mission has a coast period lasting several years. During this period, the reactor would be powered down, and the radiators would be relatively cool. By adjusting the spacecraft axis so that the tank faces away from the sun, the tank can radiate to space, thereby eliminating the need for cooling by venting gas. The tank is isolated from the rest of the spacecraft by a thermal shield consisting of two half-circle disks of 2.4 m radius and a rectangular plate 4.8 m long by 2.6 m wide. The mass of these shields totals 27 kg,

Table 2 Propellant storage component masses

Component	Mass, kg
Tank, 7.0 m^3	90.0
Multilayer insulation	66.0
Structure	169.0
Propellant acquisition device	21.0
TVS/VCS	16.0
Burst relief valve (1)	1.7
Remote operator valve (2)	5.2
Latch solenoid (2)	0.7
Pyro valve (4)	1.3
Pressure regulator (2)	3.4
Pressure sensor (4)	1.2
Heater (1)	0.2
Lines	2.0
Thermal shields	27.0
Total	404.7

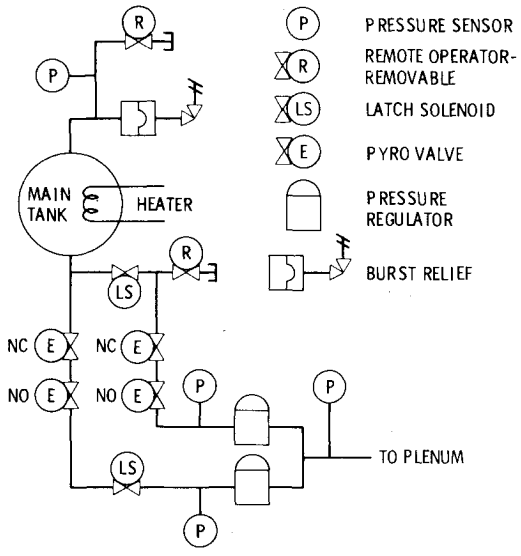

Fig. 6 Propellant storage schematic.

including support structure (see Table 2). With these shields in place, the propellant tank heat load drops to 12 mW, assuming it is proportional to the temperature drop between the exterior and the interior of the tank. This heat load is easily radiated away by the exposed tank area; thus, the vent rate during the coast phase drops to zero.

Injection

The technical difficulties in developing an appropriate propellant pulse shape at the thruster far outweigh the difficulties in providing an appropriate discharge current pulse due to the relative ease of electrical pulse shaping. Thus, for this study, the thruster discharge pulse shape and duration will be chosen based on an assessment of the propellant injection valve capabilities. Various high-speed valve concepts have been developed in the past; however, relatively few have been designed to meet the stringent reliability, temperature, and lifetime requirements needed for the MPD thruster system. Perhaps the most well understood valve design is the simple solenoid valve. Recent laboratory testing has shown that a simple off-the-shelf industrial solenoid valve can be driven to develop sinusoidal gas pulses as short as 2 ms.[12] Improved versions of such a valve are expected to be able to provide trapezoidal gas pulses to the thruster discharge chamber with rise and fall times as short as 0.3 ms.

Until a valve with the required performance characteristics is designed and tested with the MPD thruster, it will be difficult to make accurate assessments of its leak rate degradation with time or, more simply, its ultimate lifetime. Similar mechanical valves used to inject fuel mixtures at high temperatures are used as injectors in diesel engines and ordinarily last as long as 5×10^8 pulses. Space qualified solenoid valves have been developed with minimum lifetimes of 10^7 pulses, and certain industrial solenoid valves for aerospace applications are rated at 10^9 pulses and have lasted in situ as long as 2×10^9 pulses.[13,14] In all, it is apparent that an advanced solenoid valve for MPD thruster propellant injection can probably be developed to last up to 10^8 to 10^9 pulses.

From thermal analyses, the base of the thruster can reach a temperature of 850 K; thus, the valve used for this system will require a metallic seat and a high-temperature ceramic insulator. A preliminary examination of such a valve design has been completed and indicates that, although stringent, these valve requirements are not insurmountable. Typical existing solenoid valves are roughly 2–3 cm in diameter, 3–5 cm long, and roughly 200 g in mass. Due to the high temperature and fast response times required for this application, these valves will be estimated to mass 500 g. Six valves are required to ensure azimuthally uniform flow into the thruster and have a total mass of 3 kg. Conservatively, it will be assumed that each valve in the present design will require 10 J for a 5 ms pulse; thus, 60 J will be required per pulse in total. At a pulse rate of 4.4 Hz, 265 W will be necessary to drive the propellant valves.

From the primary propellant storage system, argon is fed into a plenum chamber immediately upstream of the high-speed valve assembly. This chamber serves as a holding tank where the steady inlet flow is buffered into a pulsed output. As such, it must be large enough to provide an approximately constant pressure source to the injector choked orifices during the pulse in order to ensure a high quality pulse shape. For this design, the plenum chamber consists of the cylindrical volume bounded by the inner radius of the PFN inductor coils and the volume bounded by the cylindrical conductors between the switch and the thruster (see Fig. 3). The total plenum chamber volume is approximately 0.44 m^3. Assuming a steady-state temperature, the plenum pressure during the thruster discharge will drop by a fraction proportional to the ratio of the discharge mass (0.011 g) to the initial mass (780 g) in the plenum, or about 0.001%. Thus, the plenum pressure is effectively constant and the thruster propellant mass flow is also constant through the entire pulse duration.

High-Current Switch

The MPD thruster system high-current switch controls the current flow between the capacitive pulse forming network and the thruster cathode. The switch must hold off the PFN charging voltage of 320 V and must conduct a rectangular pulsed current of 25 kA with an effective turn-on transient that is much less than the discharge pulse rise time of 0.3 ms. During the switch conducting phase its impedance must be minimal to prevent unacceptable losses from developing due to the large discharge current. Finally, in addition to these already stringent requirements, the switch must carry out its operation for the duration of the baselined Neptune orbiter mission for roughly 8.3×10^8 thruster discharge pulses.

Of all the previous requirements, the most stringent is the long lifetime, given the other operating parameters. The only switch types which can presently meet this lifetime requirement are transistors and silicon controlled rectifiers (SCR's). Available transistors are limited to peak currents of order 200–500 A maximum; thus for this application, a minimum of 50 parallel units would be required.[15] On the other hand, SCR's can handle over 1500 A and have been used successfully in laboratory MPD thruster systems.[16] A typical high-current SCR was chosen for use in the design of the switch for the present system. This SCR is by Westinghouse, part number T9GH-11, and is presently available as off-the-shelf hardware, with characteristics tabulated in detail in Ref. 17. It is a hockey puck design, 74 mm in diameter and 27 mm thick, with a mass of 0.908 kg.

Recognizing that the PFN capacitors are limited to a maximum temperature of 100°C, and to ensure that there is adequate margin for local hot spots, a temperature of 90°C was chosen for this design for the switch, PFN, and power processor electronics. At 90°C and 25 kA, 14 SCR's are required. Sixteen SCR's were used to provide for redundancy. These SCR's are configured in a cylindrically symmetric configuration as shown in Fig. 7. The energy dissipated per charge-discharge cycle in the total switch is 232 J for an equivalent power loss of 1022 W.

The plates which serve to clamp the SCR's into the circuit are copper, 1 cm thick. These plates are designed to provide the recommended 5000 lb compression per SCR with six insulated bolts around each SCR to ensure uniform loading. To ensure that the current is distributed uniformly among the SCR's, the total plate radial impedance from the outer to the inner edge is designed to be much less than the equivalent individual SCR impedance of 1.2 mΩ. Finally, these clamp plates are sized to provide an adequate radial thermal conduction path to maintain acceptable SCR temperatures at the

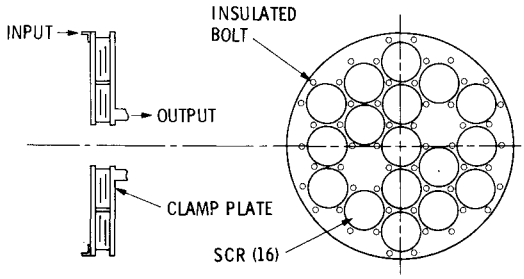

Fig. 7 High-current switch.

Table 3 High-current switch characteristics

SCR number	16
SCR mass, kg	14.5
Clamp plate mass, kg	23.0
Hardware mass, kg	1.08
Total switch mass, kg	38.58

inner radius locations, with heat pipe cooling at the switch outer diameter. The total high current switch mass breakdown is shown in Table 3.

The overall switch reliability for the required 8.3×10^8 cycles is a function of the switch junction temperature and the percentage of actual to rated forward blocking voltage. For the planned operation, the estimated individual SCR failure rate is 0.3% per 1000 h, or 16% over the system operating time of 52,000 h. Thus, of a total 16 SCR's in the switch, roughly 2–3 SCR's would be expected to fail by degradation during the total mission, assuming no stress screening prior to installation. With prior stress screening, less than one SCR should fail. From the previous design considerations, including the two redundant SCR's, the switch should be well able to support the system operation throughout the total mission.

Energy Store

During the 5 ms discharge pulse, the MPD thruster uses 20 kJ of energy. Neglecting the small losses in the switch, the energy storage components must accumulate this 20 kJ during the charging cycle and discharge it into a nominally 6.4 mΩ thruster load. For the discharge current pulse to match the propellant pulse, the energy storage output should have rise and fall times of 0.3 ms.

Background

There are a number of available options for the energy storage components of an MPD thruster system, including inductive storage, inertial storage, low-voltage capacitive circuits, high-voltage capacitive/pulse transformer combinations, and various mixed inductive/capacitive circuits that control the output pulse shape as well as store energy. Inductive storage coils have been examined for MPD applications and are being extensively studied for other applications; however, the current state-of-the-art is well away from that required for long-term space flight applications.[18] Inertial storage is just beginning to be examined for space applications after having been developed for a variety of ground uses, including industrial welding and pulsed high power fusion research.[19] Oil-filled high-voltage capacitors have the highest energy densities of any state-of-the-art components and have been flight proven in pulsed plasma thruster systems.[20] To take advantage of this high-energy density, these capacitors must be charged to high voltage (2000 V). To match this high voltage with the relatively low voltage of the MPD thruster requires an impedance matching transformer. Recent studies of this type of circuit suggest that the mass of this transformer more than offsets the gain in capacitor energy density, such that the total circuit is more massive than a low-voltage, low-energy density electrolytic capacitor PFN.[21] One of the purposes of this system study is to evaluate the design of this type of PFN to identify potential concerns and to enable a more careful comparison with alternative energy storage designs. Accordingly, electrolytic capacitors were baselined for this design study.

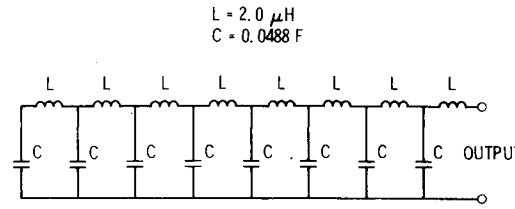

Fig. 8 PFN circuit.

Circuit

The circuit consists of an L-C ladder network where the capacitively stored energy is metered out to the thruster through inductors, which serve to regulate the pulse shape such that it follows a rectangular shape, rather than an exponential decay. The PFN circuit configuration chosen for this system design is shown in Fig. 8. As can be seen, this circuit is a repetitive series of single stages, each made up of a capacitor in series with an inductor.

The peak charging voltage of this PFN circuit is twice its discharge voltage, or 320 V for the 160 V thruster. At this voltage and for a total stored energy of 20 kJ, the required capacitance is 0.3906 F. Requiring that the PFN impedance match the load impedance of 6.4 mΩ, the inductance is 16 μH. The pulse rise time is approximately the pulse duration divided by twice the number of PFN stages. For a rise time of 0.3 ms, the number of stages for this design is eight. With this number, the necessary capacitance per stage is 48.83 mF and the necessary inductance is 2 μH.

Capacitor Characteristics

Rather than making somewhat artificial projections of electrolytic capacitor technology in order to develop capacitor specifications, an existing state-of-the-art electrolytic capacitor was used for this design. Studies have examined the various types of electrolytic capacitors and concluded that only tantalum cased, tantalum capacitors presently have the potential to meet the high reliability and lifetime requirements of this design application. Unfortunately, this type of capacitor is currently only available in relatively small unit sizes, leading to a bulky PFN design with a relatively small energy density due to excessive packaging losses. Future capacitor designs are expected to be available in much larger units with greater energy densities; thus, this disadvantage should be alleviated in time.

The particular electrolytic capacitor chosen for this PFN design is a Sprague Type 135D TANTALEX.[22,23] This capacitor has a relatively low equivalent series resistance, a high capacitance-voltage product per unit volume and an extremely low dc leakage current. Typical tantalum capacitors utilize cases made of silver, and are life limited by silver migration within the electrolyte and by loss of electrolyte through leakage. The TANTALEX capacitor chosen for this design is an all tantalum design, thereby eliminating silver migration as a life-limiting factor. This capacitor also utilizes an improved tantalum-to-glass seal which greatly reduces the concerns with electrolyte leakage. As long as known temperature and voltage limits are observed, there is presently no known failure mode for this capacitor. A series of life tests has been completed which demonstrates that the capacitor characteristics under varying temperature, ripple current magnitude, and frequency levels are stable and, in fact, track the results of 10,000-h dc bias life tests. A number of 400 Hz ac tests were continued for over 10^9 full voltage bias charge-discharge cycles, with less than a 1% degradation in unit capacitance. The largest avail-

Table 4 Capacitor characteristics

Capacitance	56 μF
Energy density	18.1 J/kg
Equivalent series resistance	0.58 Ω at 120 Hz
Leakage current	14 μA (dc)
Maximum surge voltage	116 V
Maximum ripple current	0.9 A at 120 Hz
Reverse voltage	2 Vdc
Lifetime	10,000 h or 2×10^8 pulses
Dimensions	34.1 mm long 9.5 mm diameter 4 mm leads

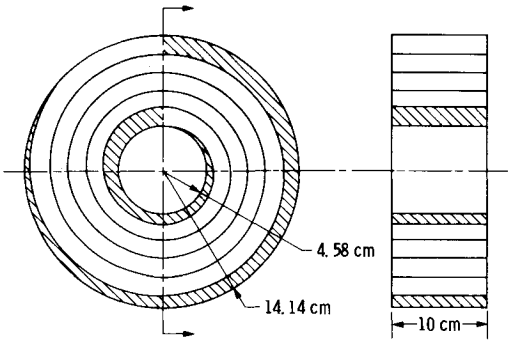

Fig. 9 PFN inductor.

able capacitor of this type is a 56 μF unit rated at 125 Vdc at 85°C or 85 Vdc at 125°C.

Reaching the design charging voltage requires that a minimum of three of these capacitors be connected in series with an individual bias of 106 V. At this voltage, and interpolating between the rated voltage-temperature data, this capacitor must remain at a temperature of no more than 100°C. Table 4 lists the capacitor's relevant characteristics at this design temperature. Each series-connected three-capacitor leg has an effective capacitance of 18.6 μF and can store 0.952 J at 320 V. To provide the PFN stage capacitance of 48.83 mF requires 2625 of these capacitor legs in parallel. With eight PFN stages, 21,000 legs, or 63,000 capacitors, are required in total. This large number of capacitors graphically illustrates the desirability of larger unit sizes.

The 2625 legs of capacitors in each stage are packed in a hexagonal arrangement with a 2063 cm^2 cross-sectional area. The overall length of each stage is 10.6 cm and includes the copper plates required to connect the legs in parallel, the lead wire overlap, and the required insulator. Energy losses in this stage are comprised of conductor resistance, capacitor leakage, and dissipation due to equivalent series resistance.

The overall PFN geometry was chosen to be cylindrical (see Fig. 3) for a number of reasons. This geometry tends to minimize stray inductance effects and confines all but the main inductor magnetic field to the interior volume. The main inductor magnetic field in this geometry is coaxial with the thruster. This cylindrical design minimizes the distance from the centerline to the exterior, which improves the overall thermal conduction to the radiator heat pipes located around the exterior. Finally, this design incorporates efficient pressure vessel characteristics which allow the entire PFN to be pressurized to minimize capacitor failures due to vacuum outgassing. The overall length of the PFN is roughly 85 cm. The diameter is set by the required capacitor cross-sectional area of 2063 cm^2 and the inductor outer diameter.

Inductor

Each PFN stage has an inductor coil with an inductance of 2 μH, a length of 10 cm, and a resistance that is small compared to one-eighth of the load resistance, i.e., 0.8 mΩ. This resistance requirement not only serves to minimize the PFN losses, but also is necessary to ensure that the PFN output pulse meets the design requirements. Copper was chosen as the coil material because of its low resistivity. With the configuration shown in Fig. 9, each coil has a resistance of 0.026 mΩ, leading to a total PFN inductor resistance of 0.21 mΩ or 3.2% of the load impedance. This particular coil design has four turns, a mean radius of 9.36 cm, and an outer radius of 14.14 cm. The crosshatched areas shown in Fig. 9 represent specially shaped copper connecting links used to tie each of the eight coils together with a minimum resistance and shaped in a way that maintains the cylindrically symmetric design. These connecting links are such that the outer radius link segment on one coil connects to the inner radius segment on its adjacent coil through a flat circular plate, 0.6 cm thick, positioned between the coils. Figure 3 helps to illustrate this connection by showing an axial cross section of the PFN through the coil midplane. In the overall coil design, a layer of electrical insulation is placed between adjacent coil layers and at each coil end. For an insulator with a typical breakdown voltage strength of 200–300 V per mil, 0.0127 cm is more than adequate for anywhere in this PFN design. The total coil mass, including connecting links and insulation, is 423.9 kg.

Assembly Details

To minimize the overall circuit inductance between the PFN inductor output and its anode return lead, the anode lead is designed as a cylinder concentric with the PFN inductor and separated from it by only a thin electrical insulator. This cylinder has a mass of 13.6 kg and a negligible electrical resistance of 10^{-3} mΩ. To provide support for the PFN capacitors surrounding the inductor coil, this anode cylinder is divided into eight equal segments, with bolt flanges at the end of each segment.

Figure 10 is a cross-section schematic of a single PFN stage showing the layout of the inductor and the anode cylinder bolt flanges. Also included in this schematic are the anode and cathode radial capacitor support plates, equipotential plates, outer cylinder wall, and the fuse link connectors between the capacitor cathode plates and the inductor coil. These fuse links provide for short circuit protection in the unlikely event that one or more capacitors fails and becomes a short circuit. Each of the eight PFN stages is hexagonally divided into six separate segments, which are individually fused between their separate cathode plates and inductor connections. With this arrangement, the PFN is divided into 48 separate segments such that only a small fraction of its capability is lost if one segment fails.

The PFN outer cylinder wall is electrically connected to the anode lead of the PFN, defined as the thruster system electrical ground. This outer wall is sized to support a PFN internal pressure of 10 atm and consists of eight 0.1 cm thick copper wall segments 10.4 cm long, with flanges at each end. Each of these segments fits between a pair of radial anode plates which are clamped to these segments between adjacent flanges, as shown in Fig. 10.

Circuit Currents

The total efficiency of the PFN and the heat generated within it can be calculated by considering the sum of all the resistive losses in its components during a full charge/discharge cycle. These losses can be calculated accurately only if the total current through each component is known as a function of time. During the charging phase, the total power input is constant and assumed equal to 100 kWe. Constant power charging is most efficient in terms of power supply utilization, but demands extremely high currents when the PFN voltage is low. For this design, the charging power processor will be assumed to be current limited to 3125 A, corresponding to a voltage of 32 V at 100 kWe. At 3125 A

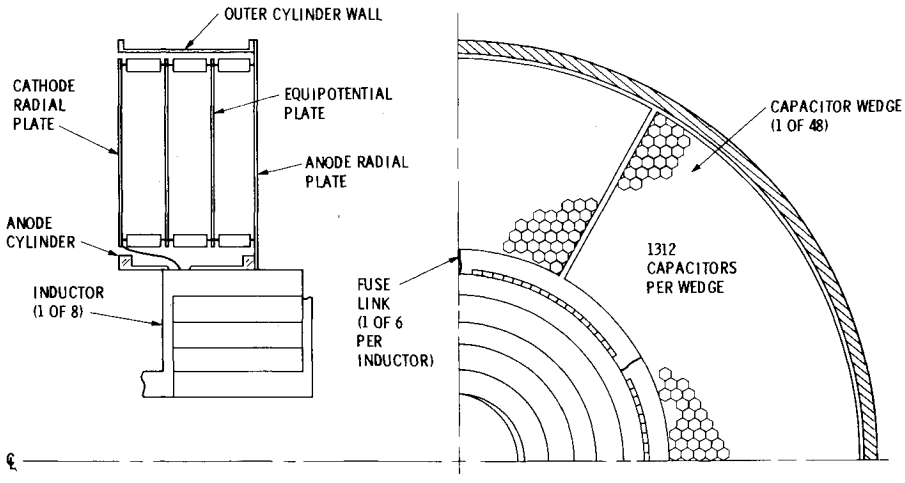

Fig. 10 PFN stage schematic.

input, the PFN requires roughly 4 ms to charge from 0 to 32 V. Once at this voltage, the power processor can proceed with constant power charging for the remaining 218 ms of charging time.

The rms time average current during the charging phase is 675 A, while the peak rate of change of current with time does not exceed 10^6 A/s. Each PFN inductor will develop no more than 0.1 V due to its resistance and no more than 2 V due to its reactance. These low inductor voltages indicate that the charging current distributes itself relatively uniformly between each of the PFN capacitors. Thus, the rms time averaged charging current into each stage is 84.3 A. During discharge, the current is taken as 25 kA for each inductor. In fact, the inductor currents should decrease from 25 kA at Stage 1 to roughly 17 kA at Stage 8; however, for simplicity and to ensure adequate design margin in the thermal analysis, the larger constant value will be used. The capacitors discharge into the inductor line in phase with a traveling wave moving from Stage 1 to Stage 8 and then reflecting back to Stage 1. The Stage 8 capacitor discharges an rms current of 17.6 kA for 0.625 ms. The remaining capacitors discharge in two pulses, one each time the traveling wave passes. Each pulse is 0.625 ms in duration with an rms current of 8.8 kA.

Thermal Analysis and Radiator Design

The entire MPD thruster system subassembly, comprised of the PFN, high current switch, propellant plenum chamber, and thruster, was analyzed to determine the heat and temperature distributions within it. This analysis was carried out iteratively with the subassembly design to ensure that the necessary heat flow to the design heat pipe radiators could be maintained with acceptable component temperatures. To simplify this analysis, the subassembly was artificially split into various regions which were analyzed separately and then pieced together by matching boundary conditions. Each region was analyzed with a one-dimensional model that allows for varying conduction areas, radiative cooling perpendicular to the primary heat flow, and ohmic heating in the conductor material. The following paragraphs describe the thermal analyses of the PFN, switch, thruster, and plenum chamber, respectively. The final paragraph discusses the heat pipe radiator design developed for this system.

The heat generated in each inductor and capacitor section in the PFN was calculated along with generation in conductors and fuses. The heat flow was simplified for analysis by realizing that the predominant conduction direction would be radial in each capacitor section and axial along the series of inductors. These assumptions are conservative for design purposes, since they will predict slightly larger thermal impedance within the PFN than would follow from a more complex analysis. The results of this analysis show that the peak capacitor temperature occurs in the centermost portion of the PFN and is 101.5°C when the outer case of the PFN is kept at 90°C. The generation of heat in the inductors results in an axial flow to the switch of 1260 W.

Given the heat flow from the PFN inductor to the switch as a function of switch temperature, it is possible to calculate the radial temperature profile in the switch. The heat generated in the switch arises from losses in the SCR switching elements and is uniformly distributed over the switch area. This internally generated heat and the input from the PFN inductor is conducted radially outward in the switch clamp plates to a radius of 14 cm, where it is directly coupled to a 90°C heat pipe. The average switch temperature is within 2–3 deg of 90°C as required by the switch design analysis.

The total heat load into the thruster is confined primarily to the anode, and is conservatively assumed to be 10 kWt. This heat flow originates from the discharge heat input and flows radially outward and axially upstream in the anode material. A major portion is radiated to space from the outer anode surface and downstream face. The remainder flows upstream through the plenum chamber walls. Portions of this heat can eventually reach the high current switch, causing an increase in switch temperature and an additional load on the heat pipe radiators. To minimize this effect, the heat flow upstream must be minimized by maximizing the thruster thermal radiation. This, in turn, requires that the thruster anode be at as high a temperature as possible, consistent with material limits. For tungsten, the limiting temperature can be well over 1800 K.

A major limit on the attainable anode operating temperature arises from the close thermal coupling between the anode and the high-speed propellant valves mounted on the thruster baseplate. Practical valve materials (especially valve seats) are limited to temperatures no higher than 600°C, or roughly 870 K. Therefore, as a conservative limit, the thruster thermal design was configured to have a base plate temperature no greater than approximately 850°K. This low temperature, combined with the desired high radiative temperatures at downstream anode locations, indicates that a steep anode axial temperature gradient is necessary. To minimize the upstream heat flow with such a gradient, the anode cross-sectional conducting area should be small. For the present design, the temperature of the anode downstream face reaches 1200 K, the anode surface radiates 8334 W, and only 1766 W of heat is conducted to the plenum chamber outer wall.

The plenum geometry is configured such that the heat flow from the thruster to the cathode lead is zero. The heat from the anode is largely radiated to space from the exposed plenum chamber wall such that relatively little heat from the thruster actually reaches the switch heat pipes. The thickness

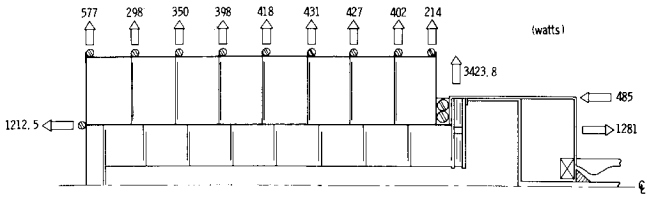

Fig. 11 Heat flux distribution.

and length of the plenum wall between the hot thruster and cool switch can be adjusted to govern the amount of heat conducted to the switch, the heat radiated to space, and the heat generated by ohmic losses in the walls. By searching for a minimum mass solution, a plenum geometry was obtained that weighs 13.77 kg, conducts 1183 W to the switch, and incurs 698 W of ohmic heating.

Based on the thermal analyses, the total heat load distribution to the heat pipe radiators is shown numerically in watts in Fig. 11. As is evident, the major heat load to the heat pipes occurs between the PFN and switch, where heat from the PFN, switch, plenum chamber, and thruster accumulates. For this switch region, two heat pipes are used at each azimuthal location due to the large heat flux and limitations on heat pipe design. These particular heat pipes were sized according to Ref. 24, which discusses a high capacity heat pipe 3 cm in diameter, capable of handling a load of 3800 W/m. For this application, the heat transfer distance is roughly 2 m; therefore, each pipe can carry up to 1900 W.

References 25 and 26 describe axially grooved heat pipes capable of supporting up to 100 W/m. Using ammonia as a working fluid, these pipes have evaporator sections from 15 to 45 cm long, and adiabatic lengths of up to 1 m. These pipes are shown in Fig. 11 for all locations other than at the PFN-switch interface. These heat pipes are all configured to support evaporator temperatures of 90°C and typically have a 5°C temperature drop from evaporator to condensor.

Rather than carrying out a detailed analysis of the heat pipe radiator design, a simple extrapolation of an existing ion thruster radiator design was made. The 30-cm ion thruster system utilizes heat pipes to cool a 50°C input using 38°C radiators. The specific mass of this radiator assembly is 23 kg/kWt, while its specific area is 2.12 m^2/kWt.[27] From the previous discussion, it is evident that heat pipe technology is well able to handle temperatures up to 100°C; thus, an extrapolation of these ion thruster radiator characteristics should be reasonably accurate. Assuming a 90°C heat pipe input requires the same end to end temperature drop as does the ion thruster design (12°C), the radiator temperature should be 78°C. Using a fourth-power scaling of temperature from 38°C to 78°C, and assuming an environmental temperature of 200 K gives the baseline MPD system radiator characteristics of 14.2 kg/kWt and 1.3 m^2/kWt. From the previous analyses, the thruster/switch/PFN subassembly generates 8.15 kWt of heat which is delivered to the heat pipe radiators. This requires a radiator assembly mass of 115.9 kg and an area of 10.6 m^2.

Power Processing

This study has concentrated on those aspects of the MPD thruster system that are significantly different from those in other electric propulsion systems. The PFN charging power processor is relatively similar to other power processors and so was not designed in detail in this study. To estimate the mass and volume of this power processor, recent literature discussing existing and future power processor technologies was reviewed and conservative extrapolations were made.[27-29] Based on these extrapolations, the power processor specific mass for this MPD thruster system design is taken to be 2 kg/kWe. Its specific volume is projected to be roughly 200 kWe/m^3 and its efficiency is 95%. The PFN power processor input is 101.2 kWe; thus its mass is 202.4 kg. The system control power processor input is 0.43 kWe; thus its mass is 0.9 kg. The total combined power processor volume is 0.5 m^3. The power processor losses are 5.1 kWt, requiring an additional radiator mass of 73 kg and an area of 6.6 m^2.

To check the projected mass and volume of the PFN power processor, a preliminary design was completed. This design used a resonant tank circuit to charge the capacitor bank from 0 to 320 V from the 200 Vdc power source. After sizing the tank circuit parameters at 50 kHz, the mass of the capacitors, magnetics, thyristors, rectifiers, and heat pipe cooling system was estimated. The mass and volume of these major components of the power processor falls well under the projections. This preliminary design indicates that hardware can be built to meet the charging requirements within the projected mass, volume, and efficiency bounds.

Summary and Potential Improvements

The system design component masses are summarized in Table 5, where it can be seen that the pulse forming network is by far the most massive component, comprising over 75% of the total system mass. The system power losses include all that is not provided directly to the thruster discharge. Table 6 summarizes these losses for the design system. Virtually all these power losses arise from ohmic losses characteristic of the high current levels required. These ohmic losses can be reduced somewhat by increasing the electrical conductor cross sections and, hence, the system mass. The current design represents a compromise between these conflicting requirements; however, no specific optimization procedure was followed to determine the most desirable combination of efficiency and mass for this particular spacecraft application. As is evident in Table 6, the PFN is the largest single contributor to the system losses.

The overall system electrical efficiency is defined as the power delivered to the thruster divided by the overall system input power and is roughly 86%. The total system efficiency is the product of this electrical efficiency and the MPD thruster thrust efficiency of 60% and is 52%. The system specific mass, given by the ratio of the total system mass to the total input power, is 21.6 kg/kWe. The system propellant storage and handling component masses are excluded from the previous

Table 5 MPD system mass summary

Component	Mass, kg
Thruster	51.3
Plenum chamber	13.86
High-current switch	38.58
PFN	1663.0
System control	29.92
Power processor	203.26
Cabling	5.0
Radiators	199.5
Total	2204.4

Table 6 MPD system losses

Component	Power, W
Thruster	41.3
Plenum chamber and propellant valves	921.8
High-current switch	1,022.0
PFN	5987.5
System control	411.2
Power processor	5,081.6
Cabling	405.0
Total	13,870.4

Table 7 MPD system overall characteristics

Average thrust	2.7 N
Specific impulse	5000 s
Average propellant flow rate	0.056 g/s
Average input power	101.87 kWe
Thrust efficiency	60%
Electrical efficiency	86%
Total system efficiency	52%
Specific mass	21.6 kg/kWe
Radiator area	18.3 m^2
Propellant storage tank fraction	4.43%

specific mass calculation, since they are typically treated separately as a percentage of the total propellant mass. The individual component masses, summarized in Table 2, total to 404.7 kg for a 9116-kg cryogenic argon propellant load; thus, the overall tankage fraction is 4.43%. The overall MPD thruster system characteristics are shown in Table 7.

The MPD system characteristics estimated in this study represent those which, except for the thruster, are consistent with present-day technology, and thus are relatively conservative. Of these technologies, the one with the greatest impact on this system design is the high-speed valve. For this design, this valve was taken as capable of no faster than a 5 ms pulse. For a peak thruster power of 4 MWe, this pulse length requires 20 kJ of energy storage in the PFN. This large energy level drives the PFN mass up to a significantly larger value than would otherwise be required. If the high-speed valve were capable of a 1 ms pulse, the energy stored would drop to 4 kJ. This in turn would lead to a drop of a factor of 5 in the required PFN capacitance and inductance, thus reducing the PFN mass significantly. The allowable PFN resistance would also drop, driving the required conductor mass up; however, the net effect would be a reduction in the PFN mass from 1663 kg to roughly 575 kg. This would reduce the overall system specific mass from 21.6 kg/kWe to 10.9 kg/kWe. Such an improvement is sufficiently significant to justify considerable effort in the area of high-speed valve development.

Other areas of potential improvement in the system design include elimination of the high-current switch and trigger circuit, improved capacitor packaging, and use of aluminum rather than copper conductors. The MPD thruster is nonconductive until propellant gas is admitted to the discharge chamber; thus, the need for a switch in series with the thruster and a trigger circuit is questionable. Recent tests using a 320 V electrolytic bank directly coupled to the thruster have shown that repeatable, reliable thruster operation is initiated on the rising edge of the mass flow pulse without a switch or a trigger discharge. By eliminating the switch and trigger circuit, the system specific mass would drop slightly and the overall power losses would be reduced by roughly 10%. The system reliability would also increase because of the considerable reduction in overall complexity. The PFN design for this system utilizes the largest currently available tantalum electrolytic capacitors because of the overall system lifetime requirements. Even so, the PFN is almost unacceptably complex due to the enormous number of single capacitor units required. Considerable simplification in the PFN design, along with a reduction in mass would be possible with larger capacitor units. By increasing the capacitance available per unit by a factor of ten, the total capacitor number would drop to 6300, or roughly 788 per PFN stage. The mass associated with casing and leads would also be reduced such that the effective capacitor energy density would increase from 24.8 to about 34 J/kg and the PFN mass would drop by roughly 300 kg. Finally, replacing copper with aluminum conductors of equal resistance would drop the total conductor mass by roughly 50% at the expense of increasing the required conductor volume by 30%.

Although the MPD thruster system design discussed in this report represents a level of detail greater than any other previous study, it does not solve or even address a number of concerns which must be resolved prior to actual assembly of a breadboard system. This design study does provide a relatively conservative assessment of the system mass and efficiency, based on short-term extrapolations of existing technology. This assessment can be useful in studies of MPD thruster applications, including deep space and near Earth missions. In addition, it can serve as a baseline to which comparisons of other electric propulsion systems can be made. Finally, the technologies identified in this study as needing further development serve as guidelines for future MPD thruster system development. Within the context of the overall MPD thruster system development program, the results of this and other studies will, it is hoped, evolve into a complete system design suitable for a variety of future space applications.

References

[1]Huberman, M., Zafran, S., Gran, H., Pieper, R., and Sellen, J.M., "Solid Teflon Pulsed Plasma Propulsion System Mission Integration Study," AIAA Paper No. 81-0729, April 1981.

[2]Rehder, J.J. and Wurster, K.E., "Electric vs. Chemical Propulsion for a Large-Cargo Orbit Transfer Vehicle," *Journal of Spacecraft and Rockets*, Vol. 16, May-June 1979, pp. 129–134.

[3]Pawlik, E.V. and Vondra, R.J., "MPD Thruster Development," AIAA Paper No. 82-1882, Nov. 1982.

[4]Nock, K.T., "Nuclear Electric Propulsion Implications," Phase II Final Report of Advanced Power and Propulsion Study, Report No. 725-71, Jet Propulsion Laboratory, Pasadena, Calif., July 1981.

[5]Burton, R.L., Clark, K..E., and Jahn, R.G., "Thrust and Efficiency of a Self-Field MPD Thruster," AIAA Paper No. 81-0684, April 1981.

[6]Saber, A.J. and Jahn, R.G., "Anode Power Deposition in Quasi-Steady MPD Arcs," AIAA Paper No. 73-1091, Nov. 1973.

[7]Mead, F.B., Jr. and Jahn, R.G., "Scaling of MPD Thrusters," AIAA Paper No. 79-2075, Nov. 1981.

[8]King, D.Q., Clark, K.E., and Jahn, R.G., "Effect of Choked Flow on Terminal Characteristics of MPD Thrusters," AIAA Paper No. 81-0686, April 1981.

[9]Esker, D.W., Kroutil, J.C., and Checkley, R.J., "Radiation Cooled MPD Arc Thrusters," NASA CR-72557, July 1969.

[10]Shadov, V.P., Porotnikov, A.A., Rylov, Ju.P., and Kim, V.P., "On Plasmajet Engine Problems and Development," Paper No. 79-06, Thirtieth International Astrophysical Congress of the IAF, Munich, Germany, Sept. 1979.

[11]Eberhardt, R.N., Fester, D.A., and Aydelott, J.C., "Shuttle Compatible Cryogenic Liquid Storage and Supply Systems," AIAA Paper No. 81-1509, July 1981.

[12]Jones, R.M., "Propellant Injection for MPD Thrusters," AIAA Paper No. 79-2074, Nov. 1979.

[13]Reinicke, R.H. and Sims, J.C., "Design and Performance of a Unique 10^7 Cycle Life Pulse Valve," AIAA Paper No. 79-1330, June 1979.

[14]Lee Interface Fluidic Miniature Solenoid Valve, The Lee Company, Westbrook, Conn.

[15]Mullin, J.P., Randolph, L.P., and Hudson, W.R., "Future Space Power—The NASA Research Perspective," AIAA Paper No. 80-0871, May 1980.

[16]Posta, S.J. and Michels, C.J., "20kA PFN-Capacitor Bank with Solid-State Switching," *Review of Scientific Instruments*, Vol. 44, Oct. 1973, pp. 1540-1541.

[17]Murphy, P.J. III, ed., *Power Semiconductor User's Manual and Data Book*, 2nd Ed., Westinghouse Electric Corp., Youngwood, Penn., Jan. 1980.

[18]Rudolph, L.K. and Jones, R.M., "Inductive Energy Storage for MPD Thrusters," AIAA Paper No. 79-0883, May 1979.

[19]Weldon, W.F., "A Study of the Applicability/Compatibility of Inertial Energy Storage Systems to Future Space Missions," Final Report, Jet Propulsion Laboratory Contract 955679, Center for Electromechanics, University of Texas at Austin, Austin, Texas, 1981.

[20]Ramrus, A., "Development of a High Energy Density Capacitor for Plasma Thrusters," Final Report, AFRPL-TR-80-35, Maxwell Laboratories, Inc., San Diego, Calif., Oct. 1980.

[21]Gabriel, S.B., "Energy Storage Systems for MPD Thrusters,"

AIAA Paper No. 81-0142, Jan. 1981.
[22]"Tantalum-Cased Tantalum Capacitors with True Glass-to-Tantalum Hermetic Seal," Sprague Engineering Bulletin 3760A, Sprague Electric Company, North Adams, Mass., 1978.
[23]England, W.F., "Tantalum-Cased Wet-Slug Tantalum Capacitors," Sprague Electric Company, North Adams, Mass.
[24]Alario, J., Edelstein, F., and Haslett, R., "Radiator Concepts for Future Space Systems," AIAA Paper No. 78-1677, Sept. 1978.
[25]Schlitt, K.R., Brennan, P.J., and Kirkpatrick, J.P., "Parametric Performance of Extruded Axial Grooved Heat Pipes from 100° to 300°K," AIAA Paper No. 74-724, July 1974.
[26]Kamotani, Y., "Effects of One-Sided Heat Input and Removal of Axially Grooved Heat Pipe Performance," AIAA Paper No. 77-191, Jan. 1977.
[27]Byers, D.C., Terdan, F.F., and Myers, I.T., "Primary Electric Propulsion for Future Space Missions," NASA TM-79141, 1979.
[28]Martinelli, R.M. and Ahrens, A.F., "Multiphase Capacitor-Diode Voltage Multiplier," IEEE Paper No. CH1337, May 1978.
[29]Bauer, D.P., Barber, J.P., and Vahlberg, C.J., "The Electric Rail Gun for Space Propulsion," NASA CR-165312, Feb. 1981.